Organic & Biomolecular Chemistry

Accepted Manuscript

This article can be cited before page numbers have been issued, to do this please use: S. Mah, J. Jang, D. Song, Y. Shin, M. Latif, Y. Jung and S. Hong, *Org. Biomol. Chem.*, 2018, DOI: 10.1039/C8OB02874E.

ROYAL SOCIETY OF CHEMISTRY

rsc.li/obc

View Article Online
DOI: 10.1039/C8OB02874E

Journal Name

ARTICLE

Discovery of Fluorescent 3-Heteroarylcoumarin Derivatives as Novel Inhibitors of Anaplastic Lymphoma Kinase

Received 00th January 20xx,
Accepted 00th January 20xx

DOI: 10.1039/x0xx00000x

www.rsc.org/

Shinmee Mah,[a,b] Jaebong Jang,[b] Daesun Song,[a] Yongje Shin,[a,b] Muhammad Latif,[b] Yongwon Jung,*[a] and Sungwoo Hong*[b,a]

Altered expression or hyperactivation of anaplastic lymphoma kinase (ALK), as a consequence of translocations or point mutations, is one of the main oncogenic drivers in non small cell lung cancer. Using structure-based design and *in vitro* enzyme assays, we identified 3-heteroarylcoumarin as a new template for the development of novel fluorescent ALK inhibitors. Molecular simulation provided structural insights for the design of 3-heteroarylcoumarin derivatives, which were easily prepared through efficient synthetic approaches including direct C-H cross coupling. Importantly, these coumarin-based ALK inhibitors can be tracked using microscopy techniques: we illustrated the use of the most potent compound in this series, **5a**, (ALK/IC_{50} = 0.51 μM, λ_{emi} = 500 nm, ϕ_F = 0.29) to monitor its subcellular distribution pattern by confocal fluorescence microscopy.

Introduction

Anaplastic lymphoma kinase (ALK) is a receptor tyrosine kinase that belongs to the insulin receptor superfamily, and normally plays a critical role in the development and maintenance of the nervous system.[1] Constitutive activation of ALK mainly caused by translocations or point mutations has been highly associated with various human cancers such as anaplastic large cell lymphoma (ALCL),[2] non-small cell lung cancer (NSCLC),[3] squamous cell carcinoma,[4] and diffuse large B-cell lymphoma.[5] In particular, an oncogenic EML4-ALK protein, generated from the fusion of the *N*-terminal part of echinoderm microtubule-associated protein-like-4 (EML4) and the kinase domain of ALK, has been intensively studied as a therapeutic target in NSCLC. Accordingly, numerous ALK inhibitors have been reported as recently reviewed in a comprehensive fashion,[6, 7] and five ALK inhibitors including crizotinib, ceritinib, alectinib, brigatinib and Lorlatinib were approved by the US FDA (Fig 1).[8, 9] Patients have shown excellent response rates to these ALK inhibitors; however, they inevitably relapse due to the emergence of resistance.[10-14] Therefore, identification of structurally diverse ALK inhibitors is important for providing novel therapeutic options for patients harboring oncogenic ALK.[15] Recently, our group reported new 4-phenoxyquinoline-based inhibitors targeting ALK WT and the L1196M mutant through structure-based design strategy (**1** and **2**, Fig 1).[16]

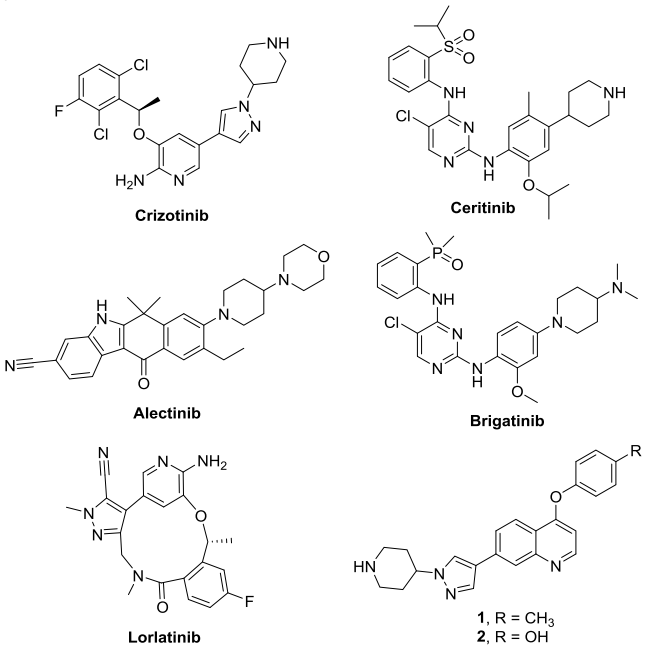

Fig 1. Chemical structures of representative ALK inhibitors.

An understanding of intracellular drug behavior such as cell membrane penetration, distribution in cells, and target engagement in biological systems is of enormous value. A tagged drug conjugated with a fluorescent dye can be broadly used to monitor the time course of drug distribution and its fate, and study biological processes in cells, animals, and humans with a noninvasive and nonradioactive procedure.[17-20] However, tethering an additional fluorescent dye in the drug molecule

[a] Department of Chemistry, Korea Advanced Institute of Science and Technology (KAIST), Daejeon 34141, Republic of Korea; E-mail: hongorg@kaist.ac.kr (S.Hong) ywjung@kaist.ac.kr (Y. Jung). Fax: 82 42 350 2810; Tel: 82 42 350 2811.
[b] Center for Catalytic Hydrocarbon Functionalizations, Institute for Basic Science (IBS), Daejeon 34141, Republic of Korea.

Electronic Supplementary Information (ESI) available: Experimental procedures, characterization data, and ^1H and ^{13}C NMR spectra for all compounds. See DOI: 10.1039/x0xx00000x

View Article Online
DOI: 10.1039/C8OB02874F

often causes negative effects on binding affinity, cell permeability, toxicity, and in vivo activity. For this reason, inherently autofluorescent drugs are more beneficial than fluorophore-conjugated compounds and can be considered as an ideal species for tracking its translocation and disposition in cells.[21-28] Coumarin constitute a major class of naturally occurring compounds, and various synthetic derivatives exhibit a broad range of biological activities as well as photophysical properties.[29-34] Therefore, significant efforts have been directed toward constructing and designing the coumarin structural motif having valuable optical properties and biological activities.[35-40] In this study, we aim to identify novel fluorescent ALK inhibitors in which the coumarin fluorophore was modified to be a pharmacophore capable of inhibiting ALK. Herein, we report studies on the identification of new coumarin-based fluorescent ALK inhibitors and demonstrate visualization of subcellular localization in living cells by fluorescence microscopy.

Results and discussion

Identification of 3-heteroarylcoumarin derivatives as fluorescent ALK inhibitors. With the goal of developing novel fluorescent ALK inhibitors, we initiated our study by testing fluorophore derivatives in our in-house coumarin-based library which was constructed by the direct cross-coupling of a coumarin core and various heteroarenes.[30] To identify the suitable structures having both inhibitory activity and fluorescence, percent enzyme activity at 100 μM against ALK and photophysical properties were examined as a primary screen, summarized in Fig 2 and Table 1. Among these coumarin derivatives that exhibited a broad emission range over 400-600 nm, 4-methylcoumarin derivative **3a** showed desirable fluorescent efficiency but weak ALK inhibitory activity (ϕ_F = 0.46, enzyme inhibition = 15%). Compared to the 4,7,8-substituents (**3a**), substitution of an amide or phenyl group at the C3-position of coumarin led to weakening optical properties (**3b**-**3d**), albeit 3-phenylcoumarin derivative **3d** displayed enhanced ALK inhibition. A comparison of 3d with **3e**-**3h**, the C3 thiazole or benzothiazole substituted analogs, showed that installation of these groups induces a red-shift in the emission wavelength and a significant increase in quantum yield (**3f**: ϕ_F = 0.32, 3g: ϕ_F = 0.72, 3h: ϕ_F = 0.72). Furthermore, the addition of a 7-alkoxy or 7-amino substituents influences the pathway of radiative decay, resulting in an increased value of quantum yield.[41] It is remarkable to note that the installation of 7-amino substituent improved the inhibitory activities with respect to ALK. Because **3h** displayed promising potency against ALK and good photophysical properties among tested coumarin analogs, **3h** was selected as a promising starting point for the development of new fluorescent ALK inhibitors.

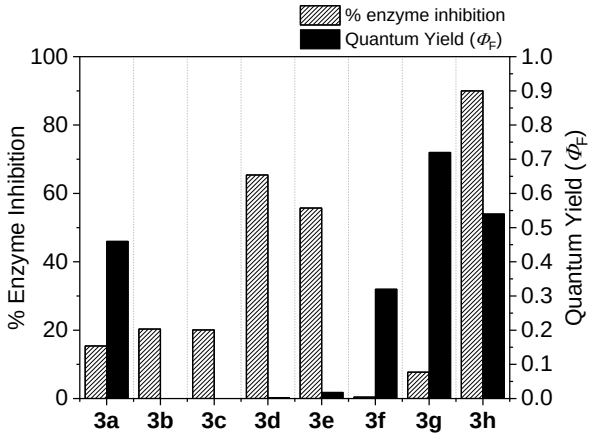

Fig 2. Percent enzyme activity at 100 μM and fluorescence quantum yield of coumarin derivatives.

Table 1. Structures and absorption/excitation wavelength of coumarin derivatives.

Compd	Structure	λ_{abs}[a] (nm)	λ_{emi}[b] (nm)
3a	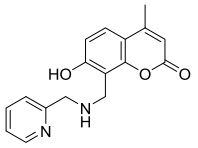	324	435
3b	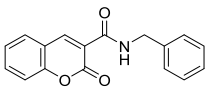	295	N.D.[c]
3c	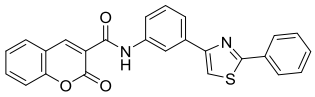	256	N.D.[c]
3d	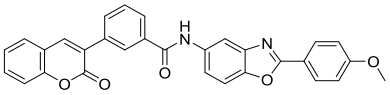	326	403
3e	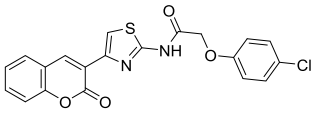	305	460
3f	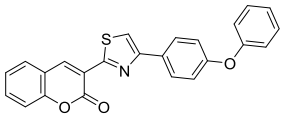	383	538
3g	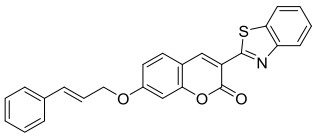	394	469
3h	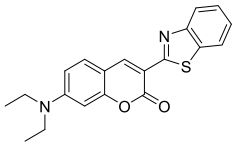	446	494

[a] Only the longest absorption maxima are shown. [b] Excited at the maximum excitation wavelength. [c] N.D. = not detected.

As a strategy to increase potency, we initially explored the C3 substituent space on coumarin and designed several 3-heteroarylcoumarin derivatives. To obtain the structural insight into the inhibitory activities, the interaction patterns of coumarin in the ATP-binding sites of ALK were investigated in the comparative fashion. Fig 3 shows the lowest energy conformation of **3h** in the ATP binding pocket of ALK (PDB ID: 2XP2)[42] as calculated with the

DOI: 10.1039/C8OB02874E

Discovery Studio 4.5 software. Molecular simulation of **3h**-ALK complex revealed that the carbonyl oxygen of coumarin core establishes a hydrogen bond with the backbone amide group of a residue (Met1199) in the hinge region of ALK. As a check for the presence of a peripheral binding pocket nearby a catalytic lysine, the calculated binding modes in this site were analyzed in detail. Because Lys1150 is located adjacent to the 6-position of the benzothiazole subunit, maintaining a distance within 3.9 Å, we hypothesized that the introduction of a suitable hydrogen bond acceptor at the C6-position of benzothiazole might improve the overall ALK inhibitory activity. To assess this hypothesis, we installed a methoxy group into this position (**4d**), which led to a slight enhancement of inhibitory activity against ALK (**3h**, IC_{50} = 2.63 μM; **4d**, IC_{50} = 1.60 μM), indicating that this enhancement of potency most likely stemmed from the strengthening of hydrogen bonds between the inhibitor and Lys1150.

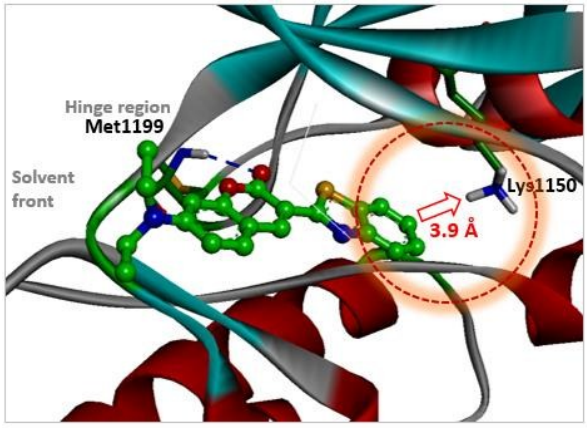

Fig 3. Calculated binding mode of **3h** in the ATP binding pocket of ALK (PDB ID: 2XP2). The blue broken line indicates a hydrogen bond. A red dotted circle shows the proximity of the C6-position of benzothiazole to Lys1150.

Optimization of ALK inhibitory activity via structure-based drug design. With respect to improving the inhibitory activity, we investigated the effect of 3-heteroaryl derivatives and substituents attached to the C7-position. For the structure-activity relationship (SAR) analysis, a survey of C3-benzothiazole analogs was conducted and IC_{50} values determined. Conversion of benzothiazole (**3h**) into benzoxazole (**4a**) showed a subtle effect on inhibitory activity but a slightly negative effect on fluorescence. Substitution of the phenyl group at the C6-position of benzothiazole (**4b**, IC_{50} = 70.9 μM) was detrimental to the potency compared with the parent molecule (**3h**, IC_{50} = 2.63 μM). A caffeine-based analog (**4c**), which also provides intense photonic luminescence, exhibited weak ALK inhibitory activity with an IC_{50} value of 39.2 μM. The negative results of **4b** and **4c** could be due to steric hindrance between the inhibitor and amino acid residues in the ALK active site. To improve the ALK inhibitory activity of **4d**, we further analyzed the structural features of the neighboring amino acids in the solvent front of the ATP binding site. The calculated binding mode of **4d** (Fig 4) revealed that the 7-diethylamino group of coumarin extends toward the solvent-exposed region and is surrounded by several amino acid residues. For example, Arg1120 is located at the upper lip of the ATP binding pocket and stretches out into the solvent exposed exterior. Interestingly, the side chain of Arg1120 shows conformational variation in several X-ray crystal structures of the ALK kinase domain: the downstretched mode of Arg1120 (Fig 4)[43, 44] could cause a putative steric clash with the rotatable diethylamine group. Based on our structural analysis, the diethylamine group was replaced with cyclic functionalities to evaluate the substituent space of the C7 position of coumarin.

Table 2. Structure-activity relationship information of 3-heteroarylcoumarin derivatives.

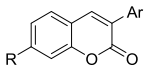

Compd	R	Ar	IC_{50} (μM)	λ_{abs}[a] (nm)	λ_{emi}[b] (nm)	ϕ_F[c]
3h		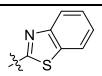	2.63	446	494	0.54
4a			2.80	433	482	0.36
4b		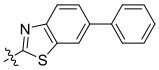	70.9	454	503	0.78
4c		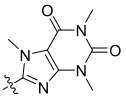	39.2	420	481	0.57
4d		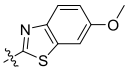	1.60	451	502	0.76
5a		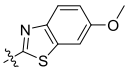	0.51	426	500	0.29
5b		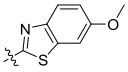	4.10	428	497	0.50
5c	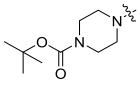	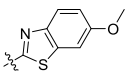	8.80	436	500	0.84
6a		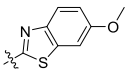	1.75	407	489	0.46
6b			22.1	379	465	0.55
6c		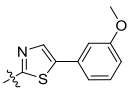	> 100	nd	nd	nd

[a] Only the longest absorption maxima are shown. [b] Excited at the maximum excitation wavelength. [c] Fluorescence quantum yield. [d] nd: not determined because of low potency.

The installation of the morpholine or piperazine moieties was intended to improve the aqueous solubility of these derivatives, which is required as a probe for real-time monitoring the cellular distribution. Of particular significance is the observation that the substitution with morpholine group yielded more potent inhibitor **5a** with submicromolar activity (**5a**, IC_{50} = 0.51 μM). According to the molecular docking study as depicted in

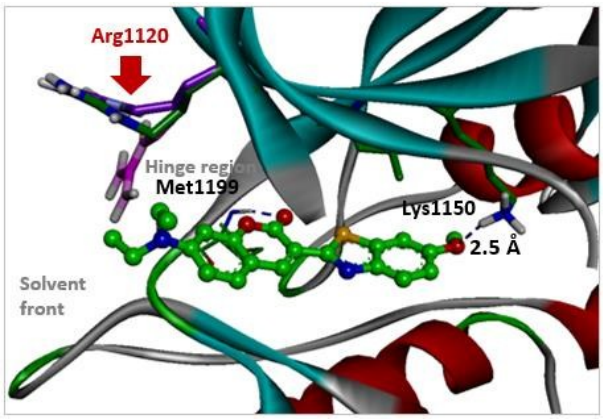

Fig 4. Predicted binding mode of compound 4d in the ATP binding pocket of ALK (PDB ID: 2XP2). Two possible locations of the Arg1120 side chain reported in PDB 3AOX[43] was superimposed.

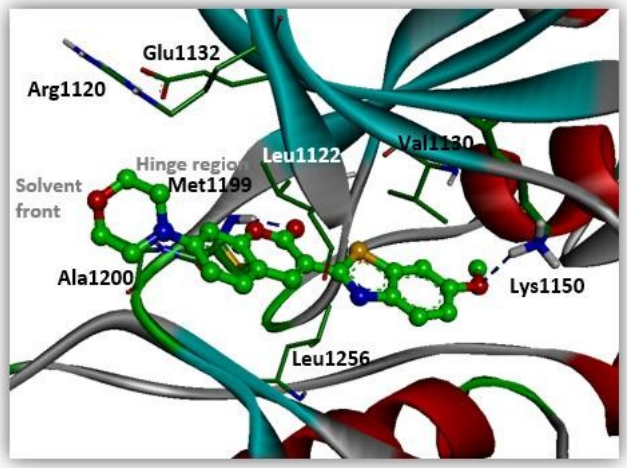

Fig 5. Predicted binding mode of compound 5a in the ATP binding pocket of ALK (PDB ID: 2XP2).

Fig 5, **5a** appears to be stabilized by multiple hydrophobic interactions with various residues including Leu1122, Val1130, and Leu1256. The improved binding affinity can be rationalized by additional hydrophobic interaction of cyclic fragment and Ala1200, Arg1120 and Glu1132 that stabilizes ligand binding. Moreover, compound **5a** showed promising fluorescence emission (**5a**, λ_{emi} = 500 nm, ϕ_F = 0.29) and Stokes shift ($\Delta\lambda \geq 70$ nm), which can be beneficial as a biological imaging study tool.[21] The enzymatic inhibitory activity of the derivatives was decreased when more sterically hindered heterocycles such as *N*-methyl or *N*-Boc piperazine moiety were introduced (**5b**, IC_{50} = 4.1 μM; **5c**, IC_{50} = 8.8 μM), indicating that the morpholine group is most suitable for this position in benzothiazole core. Replacement of the morpholine with a methoxy group resulted in reduction of inhibitory activity against ALK (**6a**, IC_{50} = 1.75 μM). The binding energy of **6a** in docking simulation was much lower than that of **5a** (**5a**, -CDocker energy = 21.8214; **6a**, -CDocker energy = 17.6135, calculated by Discovery Studio 4.5), revealing that loss of van der Waals interaction between morpholine and small pocket located in solvent front inevitably culminates in the weakening of the binding affinity of **6a**. Next, importance of the hydrogen bond network in 6-methoxybenzothiazole was further demonstrated by removal of the methoxy group (**6b**, IC_{50} = 22.1 μM). Investigation of alternate moieties such as 3-methoxyphenyl-thiazole group revealed that the 6-methoxybenzothiazole was optimal for this series, which is in turn responsible for a weaker biochemical potency of **6c** (IC_{50} > 100 μM). These results confirm the importance of forming a stable hydrogen bond of 6-methoxybenzothiazole with Lys1150 to enhance the inhibitory activity (Fig 5).

Next, the representative compounds **5a** and **6a**[45] were further tested against the most common secondary ALK mutants such as L1196M, G1269A and G1202R (Table 3). Compound **5a** showed potent inhibitory activities against three ALK mutants (L1196M IC_{50} = 0.27 μM; G1269A IC_{50} = 0.30 μM; G1202R IC_{50} = 0.59 μM). Compound **6a** displayed an IC_{50} value of 0.45 μM for L1196M and compatible enzymatic inhibitory activity against G1269A and G1202R with that against WT ALK.

Table 3. IC_{50} values of compounds against ALK WT and mutants.

Compd	ALK mutant IC_{50}[a] (μM)			
	WT	L1196M	G1269A	G1202R
5a	0.51	0.27	0.30	0.59
6a	1.75	0.45	2.30	1.82

[a] The IC_{50} measurements were performed at the Reaction Biology Corp (Malvern, PA, USA).

Monitoring molecular behavioral variability in cells by confocal microscopy. Among the fluorescent ALK inhibitors with desirable inhibitory activities, two leading compounds **5a** and **6a** were selected for further investigation of the imaging ability of its molecular behavior. Compound **5a** seems to possess more favorable physicochemical properties than **6a** based on calculated AlogP values (**5a**, ALogP = 3.70; **6a**, ALogP = 3.84, predicted by Discovery Studio 4.5 Client). In the present study, HeLa cells was used to monitor the general behavior of our fluorescent inhibitors such as cell penetration and cellular distribution. HeLa cells were incubated with **5a** or **6a** at 10 μM concentration for 1 h. Unbound compounds were washed, and the resulting cells were further incubated for 4 h and 12 h. After treatment of **5a** for 1 h, visible fluorescence was clearly detected in both plasma membrane and cytoplasm of HeLa cells, which maintained even after 12 h incubation (Fig 6). To our delight, we also observed the fluorescence at membrane region that might be evidence of membrane penetration that provided the feasibility of monitoring a time-dependent morphology change of membrane (Fig 6B and C). On the other hand, **6a** seems to be attached to cell surface plasma membrane after 1 h treatment due to the high lipophilicity. Therefore, the cell membrane penetration of **6a** appear to be inferior than that of **5a**. When the fluorescence of **6a** was monitored after 4 h or 12 h treatment, the compound was gradually distributed into the cytoplasm (Fig 7B and 7C). These results provide a visible insight of molecular behavior such as cell membrane penetration and intracellular distribution of fluorescent compounds as well as a way to monitor the cell morphology changes. The present **5a** can be used to not only functionally alter ALK activity but also monitor drug distributions, which are known to be important indicatives of various cancerous cells.

DOI: 10.1039/C8OB02874E

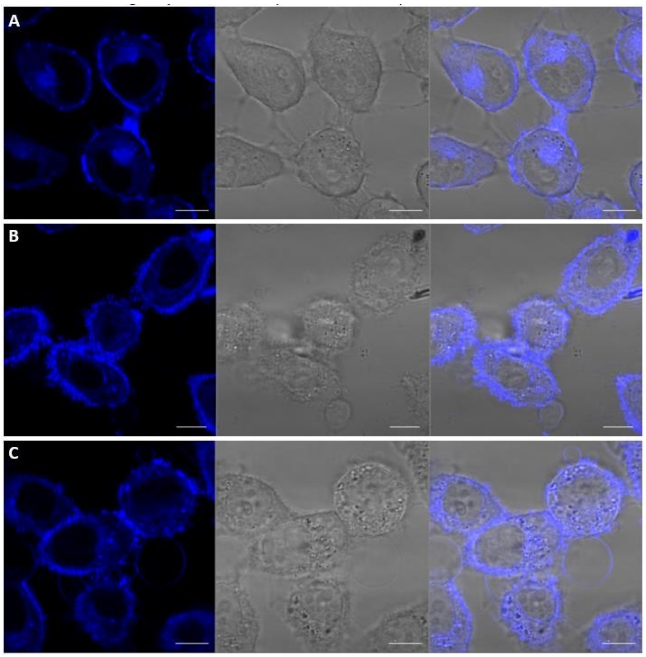

Fig 6. Confocal imaging of the intracellular disposition of compound **5a** in HeLa cells. Cells were incubated with a 10 μM solution of compound for 1 h. (A) Cells after 1 h upon treatment of **5a**. (B) Cells after 4 h upon treatment of **5a**. (C) Cells after 12 h upon treatment of **5a.** Left: transmitted light image; middle: fluorescence microscopic image; right: overlaid image. Scale bar, 10 μm

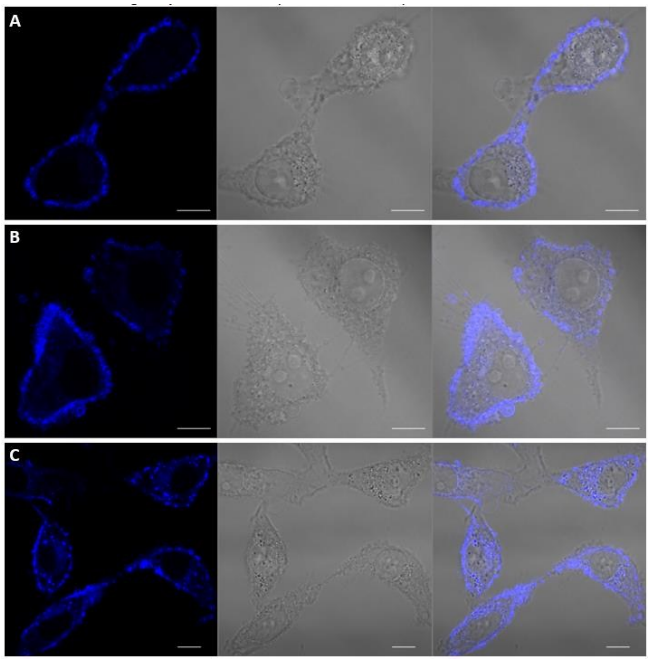

Fig 7. Confocal imaging of the intracellular disposition of compound **6a** in HeLa cells. Cells were incubated with 10 μM solution of compound for 1 h. (A) Cells after 1 h upon treatment of **6a**. (B) Cells after 4 h upon treatment of **6a**. (C) Cells after 12 h upon treatment of **6a.** Left: transmitted light image; middle: fluorescence microscopic image; right: overlaid image. Scale bar, 10 μm.

Synthesis of coumarin derivatives. Our group reported an efficient direct C–H cross-coupling approach to heteroaryl coumarins using a Pd/Cu catalytic system, which enabled the straightforward preparation of 3-heteroarylcoumarin derivatives.[30] The focused compound library was established by this synthetic method allowing for rapid exploration of the SAR profile of 3-heteroarylcoumarin derivatives (Scheme 1). To install heteroaromatic rings, the C3 position of coumarins **7** was first brominated using a mixture of oxone and hydrobromic acid in dichloromethane at room temperature, and then treating the product with Et_3N. Subsequently, various heteroaryl groups were installed at the C3 position through a Pd-catalyzed direct cross-coupling of 3-bromocoumarins with heteroarenes to afford the desired products. For compounds bearing morpholine or piperazine rings at the C7 position, the 7-fluoro-coumarin intermediate **9** was further converted to target compounds (**5a**-**5c**) using the S_NAr reactions with appropriate amines.

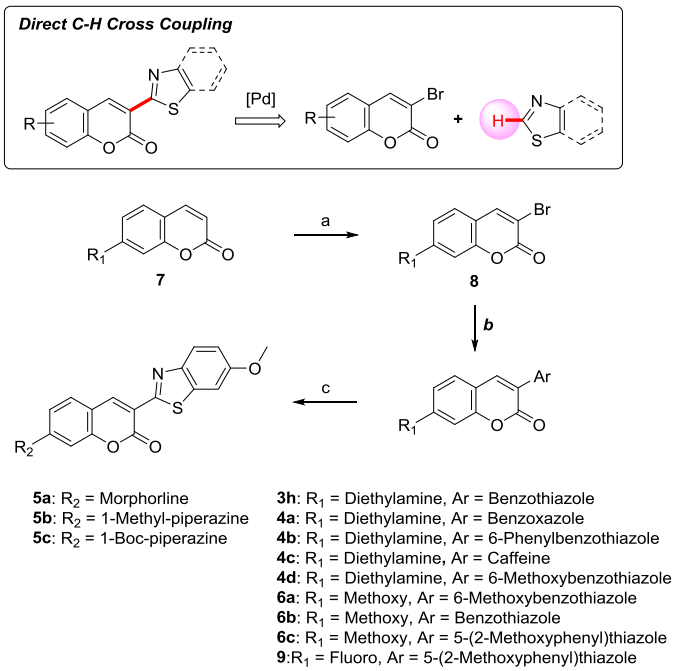

5a: R_2 = Morphorline
5b: R_2 = 1-Methyl-piperazine
5c: R_2 = 1-Boc-piperazine

3h: R_1 = Diethylamine, Ar = Benzothiazole
4a: R_1 = Diethylamine, Ar = Benzoxazole
4b: R_1 = Diethylamine, Ar = 6-Phenylbenzothiazole
4c: R_1 = Diethylamine, Ar = Caffeine
4d: R_1 = Diethylamine, Ar = 6-Methoxybenzothiazole
6a: R_1 = Methoxy, Ar = 6-Methoxybenzothiazole
6b: R_1 = Methoxy, Ar = Benzothiazole
6c: R_1 = Methoxy, Ar = 5-(2-Methoxyphenyl)thiazole
9:R_1 = Fluoro, Ar = 5-(2-Methoxyphenyl)thiazole

Scheme 1. Synthetic route for 3-heteroarylcoumarins. Reagents and conditions: (a) Oxone, 2N HBr, CH_2Cl_2, rt, 2 h, then TEA, rt, 2h; (b) Heteroarenes, $Pd(PPh_3)_4$, CuI, Cs_2CO_3, 1,4-Dioxane, 110 °C, 6 h; (c) DIPEA, Acetonitrile, 90 °C, 12 h.

Conclusions

In summary, we discovered a family of coumarin-based ALK inhibitors serving as a dual function in exhibiting fluorescence and inhibiting ALK. Guided by structure-based design and analysis of photophysical properties, we successfully identified compound **5a** with potent activity and significant fluorescence properties (ALK IC_{50} = 0.51 μM, λ_{emi} = 500 nm, ϕ_F = 0.29). Cell imaging after treatment of **5a** and **6a** showed the insight of molecular behavior such membrane penetration and intracellular distribution and provided a way to monitor cellular morphology changes such as deconstruction of lipid bilayer. The combined features of newly discovered fluorescent ALK inhibitors would be useful in biological or pharmaceutical research enabling visualization of subcellular localization in living cells by fluorescence microscopy.

DOI: 10.1039/C8OB02871F

Experimental

General

Unless otherwise stated, reactions were performed in flame-dried glassware and monitored by TLC. Analytical thin layer chromatography (TLC) was performed on pre-coated silica gel 60 F_{254} plates and compounds were visualized by UV light (254 and 365 nm). Flash column chromatography was undertaken on silica gel (400-630 mesh) and ethyl acetate, n-hexane were used as eluents for product purification. ^{1}H and ^{13}C NMR were recorded in $CDCl_3$ or CD_2Cl_2 solution on 400 or 600MHz instrument. All chemical shifts were quoted in parts per million (ppm) referenced to the appropriate solvent peak or 0.0 ppm for tetramethylsilane. The following abbreviations were used to describe peak splitting patterns when appropriate: br = broad, s = singlet, d = doublet, t = triplet, q = quartet, m = multiplet, dd = doublet of doublet, td = doublet of triplet, ddd = doublet of doublet of doublet. Coupling constant, *J* values were reported in hertz unit (Hz). Mass spectral data were obtained from KAIST Basic Science Institute by using ESI method. Commercial grade reagents and solvents were used without further purification except as indicated below.

General procedure I (GP I) for 3-bromocoumarins.

Coumarin derivative (1 equiv.) and Oxone (1.2 equiv.) were dissolved in CH_2Cl_2 (0.25 M). 2 N HBr solution (HBr 2.2 equiv.) was added and the reaction mixture was stirred at room temperature. After 2 h, Et_3N (3 equiv.) was added and stirred for additional 2 h. The reaction mixture was diluted with CH_2Cl_2 and water, and then the organic compounds were extracted by CH_2Cl_2. The organic layer was dried over Na_2SO_4 and evaporated. The residue was purified by flash column chromatography on silica gel (hexanes : EtOAc = 6 : 1) to give the desired product.

General procedure II (GP II) for 3-heteroarylcoumarins.

3-Bromocoumarin derivative (1 equiv.), heteroarene (2 equiv.), $Pd(PPh_3)_4$ (2.5 mol%), CuI (3 equiv.), and Cs_2CO_3 (2 equiv.) were combined in 1,4-Dioxane under air. The reaction mixture was heated to 110 ^{o}C with stirring, and monitored by TLC using ethyl acetate and n-hexane as the mobile phase. After disappearance of starting material, the reaction mixture was diluted and filtered through Celite with CH_2Cl_2. After removal of solvent, the residue was purified by flash column chromatography on silica gel to provide the desired product.

General procedure III (GP III) for 7-substituted 3-heteroarylcoumarins.

7-Fluoro-3-(6-methoxy-1,3-benzothiazol-2-yl)chromen-2-one (1 equiv.) was dissolved in Acetonitrile at room temperature under air. To this solution, cyclic aliphatic amines (2 equiv.) and DIPEA (3 equiv.) were added. The reaction mixture was stirred at 90 ^{o}C for 12 h. After completion of reaction, the mixture was cooled to rt. Then, the precipitate was collected by filtration with cold Acetonitrile and water to give the desired product.

3-(1,3-Benzothiazol-2-yl)-7-(diethylamino)chromen-2-one (3h). Compound **3h** was prepared (yellowish orange solid, 8.0 mg, 2 steps- 21% overall yields) according to GP I and GP II. ^{1}H NMR (600 MHz, Chloroform-*d*) δ 8.92 (d, *J* = 1.9 Hz, 1H), 8.02 (d, *J* = 8.1 Hz, 1H), 7.95 (d, *J* = 8.0 Hz, 1H), 7.49 (dd, *J* = 7.3, 4.1 Hz, 2H), 7.36 (t, *J* = 7.6 Hz, 1H), 6.68 (dt, *J* = 9.0, 2.2 Hz, 1H), 6.57 (d, *J* = 2.3 Hz, 1H), 3.47 (q, *J* = 7.4 Hz, 4H), 1.26 (t, *J* = 7.2 Hz, 6H). ^{13}C NMR (150 MHz, Chloroform-*d*) δ 161.8, 161.0, 157.0, 152.6, 152.1, 142.0, 136.3, 130.8, 126.0, 124.4, 122.1, 121.6, 112.5, 109.9, 108.7, 97.0, 45.1, 12.5. HRMS (ESI$^+$) m/z calcd. for $C_{20}H_{18}N_2NaO_2S^+$ [M + Na]$^+$: 373.0981, found: 373.0984.

3-(1,3-Benzoxazol-2-yl)-7-(diethylamino)chromen-2-one (4a). Compound **4a** was prepared (yellow solid, 8.4 mg, 2 steps- 24% overall yields) according to GP I and GP II. ^{1}H NMR (600 MHz, Methylene Chloride-d_2) δ 8.60 (s, 1H), 7.73 (dd, *J* = 5.9, 3.2 Hz, 1H), 7.59 (dd, *J* = 5.9, 3.3 Hz, 1H), 7.45 (d, *J* = 8.9 Hz, 1H), 7.34 (dd, *J* = 6.0, 3.2 Hz, 2H), 6.67 (dd, *J* = 8.9, 2.4 Hz, 1H), 6.53 (d, *J* = 2.3 Hz, 1H), 3.46 (q, *J* = 7.1 Hz, 4H), 1.23 (t, *J* = 7.2 Hz, 6H). ^{13}C NMR (150 MHz, Methylene Chloride-d_2) δ 160.1, 157.8, 157.6, 152.6, 150.4, 145.4, 142.1, 130.6, 124.8, 124.4, 119.7, 110.3, 110.0, 109.7, 108.1, 96.7, 45.1, 12.2. HRMS (ESI$^+$) m/z calcd. for $C_{20}H_{18}N_2NaO_3^+$ [M + Na]$^+$: 357.1210, found: 357.1219.

7-(Diethylamino)-3-(6-phenyl-1,3-benzothiazol-2-yl)chromen-2-one (4b). Compound **4b** was prepared (dark red solid, 8.1 mg, 2 steps- 18% overall yields) according to GP I and GP II. ^{1}H NMR (600 MHz, Methylene Chloride-d_2) δ 8.93 (s, 1H), 8.15 (d, *J* = 1.7 Hz, 1H), 8.02 (d, *J* = 8.4 Hz, 1H), 7.73 (dd, *J* = 8.6, 1.7 Hz, 1H), 7.71 – 7.65 (m, 2H), 7.52 (d, *J* = 8.9 Hz, 1H), 7.47 (t, *J* = 7.6 Hz, 2H), 7.36 (t, *J* = 7.4 Hz, 1H), 6.71 (dd, *J* = 8.9, 2.3 Hz, 1H), 6.57 (d, *J* = 2.3 Hz, 1H), 3.47 (q, *J* = 7.2 Hz, 4H), 1.24 (t, *J* = 7.1 Hz, 6H). ^{13}C NMR (150 MHz, Methylene Chloride-d_2) δ 162.0, 160.9, 157.1, 152.3, 151.9, 142.0, 140.7, 137.6, 136.9, 130.8, 128.8, 127.3, 127.2, 125.7, 122.0, 119.6, 112.1, 110.0, 108.6, 96.8, 45.1, 12.2. HRMS (ESI$^+$) m/z calcd. for $C_{26}H_{23}N_2O_2S^+$ [M + H]$^+$: 427.1475, found: 427.1488.

8-[7-(Diethylamino)-2-oxo-chromen-3-yl]-1,3,7-trimethyl-purine-2,6-dione (4c). Compound **4c** was prepared (yellow solid, 14.5 mg, 2 steps- 34% overall yields) according to GP I and GP II. ^{1}H NMR (400 MHz, Methylene Chloride-d_2) δ 8.02 (s, 1H), 7.39 (d, *J* = 8.9 Hz, 1H), 6.67 (dd, *J* = 8.9, 2.5 Hz, 1H), 6.54 (d, *J* = 2.4 Hz, 1H), 3.91 (s, 3H), 3.55 (s, 3H), 3.47 (q, *J* = 7.1 Hz, 4H), 3.36 (s, 3H), 1.24 (t, *J* = 7.1 Hz, 6H). ^{13}C NMR (100 MHz, Methylene Chloride-d_2) δ 159.7, 158.0, 155.7, 152.6, 152.0, 148.6, 148.4, 147.7, 130.5, 110.0, 109.0, 108.4, 97.2, 45.4, 34.0, 29.8, 28.0, 12.6. HRMS (ESI$^+$) m/z calcd. for $C_{21}H_{23}N_5NaO_4^+$ [M + Na]$^+$: 432.1642, found: 432.1667.

7-(Diethylamino)-3-(6-methoxybenzo[*d*]thiazol-2-yl)-2*H*-chromen-2-one (4d). Compound **4d** was prepared (yellow solid, 9.1 mg, 2 steps- 17% overall yields) according to GP I and GP II. ^{1}H NMR (400 MHz, Methylene Chloride-d_2) δ 8.83 (s, 1H), 7.86 (d, *J* = 8.9 Hz, 1H), 7.50 (d, *J* = 8.9 Hz, 1H), 7.41 (d, *J* = 2.5 Hz, 1H), 7.08 (dd, *J* = 8.9 Hz, 2.5 Hz, 1H), 6.70 (dd, *J* = 8.9, 2.5 Hz, 1H), 6.57 (d, *J* = 2.4 Hz, 1H), 3.89 (s, 3H), 3.47 (q, *J* = 7.1 Hz, 4H), 1.25 (t, *J* = 7.1 Hz, 6H). ^{13}C NMR (100 MHz, Methylene Chloride-d_2) δ 161.4, 159.6, 157.8, 157.3, 152.5, 147.7, 141.6, 138.1, 131.0, 123.1, 116.1, 112.9, 110.3, 108.9, 104.0, 97.2, 56.2, 45.4, 12.6. HRMS (ESI+) m/z calcd. for $C_{21}H_{20}N_2NaO_3S^+$ [M + Na]$^+$: 403.1087, found: 403.1092.

View Article Online
DOI: 10.1039/C8OB02874E

3-(6-Methoxy-1,3-benzothiazol-2-yl)-7-morpholino-chromen-2-one (5a). Compound **5a** was prepared (yellowish orange solid, 15.0 mg, 3 steps- 34% overall yields) according to GP I, GP II and GP III. ^{1}H NMR (400 MHz, Chloroform-*d*) δ 8.89 (s, 1H), 7.93 (d, *J* = 8.9 Hz, 1H), 7.55 (d, *J* = 8.8 Hz, 1H), 7.39 (d, *J* = 2.5 Hz, 1H), 7.12 (dd, *J* = 8.9, 2.5 Hz, 1H), 6.88 (dd, *J* = 8.8, 2.4 Hz, 1H), 6.78 (d, *J* = 2.3 Hz, 1H), 3.91 (s, 3H), 3.90 – 3.84 (m, 4H), 3.41 – 3.33 (m, 4H). ^{13}C NMR (150 MHz, Chloroform-*d*) δ 160.7, 158.5, 157.6, 156.1, 154.4, 147.2, 140.7, 138.0, 130.2, 123.0, 116.2, 115.4, 111.8, 111.0, 103.6, 100.1, 66.4, 55.8, 47.3. HRMS (ESI$^+$) m/z calcd. for $C_{21}H_{18}N_2NaO_4S^+$ [M + Na]$^+$: 417.0880, found: 417.0872.

3-(6-Methoxy-1,3-benzothiazol-2-yl)-7-(4-methylpiperazin-1-yl)chromen-2-one (5b). Compound **5b** was prepared (yellowish orange solid, 12.0 mg, 3 steps- 26% overall yields) according to GP I, GP II and GP III. ^{1}H NMR (600 MHz, Chloroform-*d*) δ 8.84 (d, *J* = 1.3 Hz, 1H), 7.91 (dd, *J* = 8.9, 1.3 Hz, 1H), 7.50 (dd, *J* = 8.9, 1.4 Hz, 1H), 7.38 (dd, *J* = 2.5, 1.4 Hz, 1H), 7.10 (ddd, *J* = 8.9, 2.6, 1.3 Hz, 1H), 6.86 (ddd, *J* = 8.9, 2.5, 1.4 Hz, 1H), 6.75 (t, *J* = 1.7 Hz, 1H), 3.90 (d, *J* = 1.4 Hz, 3H), 3.51 – 3.21 (m, 4H), 2.67 – 2.42 (m, 4H), 2.36 (d, *J* = 1.4 Hz, 3H). ^{13}C NMR (150 MHz, Chloroform-*d*) δ 160.8, 158.7, 157.5, 156.2, 154.3, 147.2, 140.8, 137.9, 130.2, 122.9, 116.1, 114.8, 112.0, 110.5, 103.6, 100.0, 55.8, 54.5, 47.1, 46.1. HRMS (ESI$^+$) m/z calcd. for $C_{22}H_{22}N_3O_3S^+$ [M + H]$^+$: 408.1376, found: 408.1383.

***tert*-Butyl 4-[3-(6-methoxy-1,3-benzothiazol-2-yl)-2-oxo-chromen-7-yl]piperazine-1-carboxylate (5c).** Compound **5c** was prepared (yellowish orange solid, 13.0 mg, 3 steps- 24% overall yields) according to GP I, GP II and GP III. ^{1}H NMR (400 MHz, Chloroform-*d*) δ 8.87 (s, 1H), 7.92 (d, *J* = 8.9 Hz, 1H), 7.54 (d, *J* = 8.8 Hz, 1H), 7.39 (d, *J* = 2.6 Hz, 1H), 7.11 (dd, *J* = 9.0, 2.6 Hz, 1H), 6.87 (dd, *J* = 9.0, 2.3 Hz, 1H), 6.76 (d, *J* = 2.4 Hz, 1H), 3.91 (s, 3H), 3.70 – 3.55 (m, 4H), 3.48 – 3.39 (m, 4H), 1.50 (s, 9H). ^{13}C NMR (150 MHz, Methylene Chloride-d_2) δ 160.6, 158.5, 157.6, 156.2, 154.4, 154.2, 147.2, 140.8, 137.8, 130.3, 122.9, 120.1, 115.9, 114.8, 112.0, 110.5, 103.5, 99.8, 79.8, 55.7, 47.0, 28.1. HRMS (ESI$^+$) m/z calcd. for $C_{26}H_{27}N_3NaO_5S^+$ [M + Na]$^+$: 516.1564, found: 516.1552.

7-Methoxy-3-(6-methoxy-1,3-benzothiazol-2-yl)chromen-2-one (6a). Compound **6a** was prepared (yellow solid, 11.0 mg, 2 steps- 33% overall yields) according to GP I and GP II. ^{1}H NMR (600 MHz, Chloroform-*d*) δ 8.94 (s, 1H), 7.94 (d, *J* = 8.9 Hz, 1H), 7.61 (d, *J* = 8.6 Hz, 1H), 7.40 (d, *J* = 2.5 Hz, 1H), 7.13 (dd, *J* = 8.9, 2.5 Hz, 1H), 6.95 (dd, *J* = 8.6, 2.4 Hz, 1H), 6.92 (d, *J* = 2.4 Hz, 1H), 3.93 (s, 3H), 3.91 (s, 3H). ^{13}C NMR (150 MHz, Chloroform-*d*) δ 164.0, 160.2, 157.9, 157.7, 155.8, 147.2, 140.7, 138.1, 130.3, 123.2, 117.1, 116.3, 113.8, 112.8, 103.5, 100.6, 56.0, 55.8. HRMS (ESI$^+$) m/z calcd. for $C_{18}H_{13}NNaO_4S^+$ [M + Na]$^+$: 362.0458, found: 362.0464.

3-(Benzo[d]thiazol-2-yl)-7-methoxy-2H-chromen-2-one (6b). Compound **6b** was prepared (yellow solid, 15.5 mg, 2 steps- 53% overall yields) according to GP I and GP II. ^{1}H NMR (400 MHz, Chloroform-*d*) δ 9.03 (s, 1H), 8.06 (d, *J* = 8.2 Hz, 1H), 7.95 (d, *J* = 8.2 Hz, 1H), 7.60 (d, *J* = 8.8 Hz, 1H), 7.52–7.48 (m, 1H), 7.41–7.37 (m, 1H), 6.93 (dd, *J* = 8.8, 2.4 Hz, 1H), 6.89 (d, *J* = 2.4 Hz, 1H), 3.90 (s, 3H). ^{13}C NMR δ (100 MHz, Chloroform-*d*) δ 164.7, 160.9, 160.1, 156.2, 151.2, 142.7, 135.9, 130.9, 126.7, 125.4, 122.2, 121.8, 115.9, 114.1, 112.7, 100.6, 56.1. HRMS (ESI$^+$) m/z calcd for $C_{17}H_{11}NNaO_3S^+$ [M + Na]$^+$: 332.0352, found: 332.0371.

7-Methoxy-3-[5-(2-methoxyphenyl)thiazol-2-yl]chromen-2-one (6c). Compound **6c** was prepared (yellow solid, 17.0 mg, 2 steps- 19% overall yields) according to GP I and GP II. ^{1}H NMR (600 MHz, Chloroform-*d*) δ 8.99 (s, 1H), 7.69 (s, 1H), 7.68 (d, 1H), 7.62 (t, 1H), 7.59 (d, 1H), 7.39 (t, 1H), 6.98 (dd, 1H), 6.95 (d, 1H). 6.93 (dd, 1H), 3.93 (s, 3H), 3.91 (s, 3H). ^{13}C NMR δ (150 MHz, Chloroform-*d*) δ 193.2, 163.9, 160.1, 159.3, 155.5, 154.9, 139.6, 135.7, 130.2, 129.7, 118.6, 116.8, 115.9, 113.6, 112.8, 112.0, 110.0, 100.5, 56.0, 55.3. HRMS (ESI$^+$) m/z calcd for $C_{20}H_{15}NNaO_4S^+$ [M + Na]$^+$: 388.0614, found: 388.0626.

Virtually screened fluorophore derivatives including **3a**-**3g** were purchased from commercial source (InterBioScreen Ltd., Chernogolovka, Russia).

Fluorescence quantum yield measurement

Fluorescence quantum yields (ϕ_F) were measured by a combination system of a spectrophotometer (UV-2600 UV/Vis Spectrophotometer, SHIMADZU Corp. and V-530 UV/Vis Spectrophotometer, Jasco, Inc.) with a fluorimeter (RF-6000 Spectro-fluorophotometer, SHIMADZU Corp. and RF-5301PC Spectro-fluorophotometer, SHIMADZU Corp.). Samples were prepared as solutions by dilution of the fluorescent compound in DMSO (Table 1, Fig 2) or CH_2Cl_2 (Table 2). Absorption λ_{max} was measured with a spectrophotometer scanning the 700-250 range wavelength while fluorescence emission λ_{max} and integrated intensity were analyzed with MATLAB R2014b and Origin2018b software. The Sample absorbance was maintained < 0.1 to minimize internal absorption. The absolute quantum yield of a known fluorescent dye – fluorescein and norharmane – was obtained to determine those of the sample precisely (fluorescein : ϕ_F = 0.925 ± 0.015 in 0.1 N NaOH aqueous solution, norharmane : ϕ_F = 0.58 in 0.1 N H_2SO_4 aqueous solution).

Intracellular monitoring study

Human cervical cancer (HeLa) cells from ATCC with fewer than 15 passages were cultured as monolayers in complete growth media, DMEM (Dulbecco's Modified Eagle medium, Gibco, USA) supplemented with 10% FBS (Fetal Bovine Serum, Gibco, USA) and 1 % penicillin–streptomycin (Gibco, USA), at 37 °C under 5% CO_2. Cells were treated with 10 μM fluorescent compounds for 1 h and washed 3 times with DPBS. Treated cells were further incubated for 4 h and 12 h in complete growth media and fixed with 4% paraformaldehyde for confocal imaging. Fluorescence images were obtained with a LSM 800 laser scanning confocal microscope (Carl Zeiss, LSM 800) using 100× oil objective lens. Optimized laser lines for **5a** (λ_{ex} 426 nm / λ_{em} 500 nm) and **6a** (λ_{ex} 407 nm / λ_{em} 489 nm) were used.

Conflicts of interest

There are no conflicts to declare.

Acknowledgements

This research was supported financially by the Institute for Basic Science (IBS-R010-G1).

Notes and references

1. T. Iwahara, J. Fujimoto, D. Wen, R. Cupples, N. Bucay, T. Arakawa, S. Mori, B. Ratzkin and T. Yamamoto, *Oncogene*, 1997, **14**, 439-449.
2. R. H. Palmer, E. Vernersson, C. Grabbe and B. Hallberg, *Biochem. J.*, 2009, **420**, 345-361.
3. M. Soda, Y. L. Choi, M. Enomoto, S. Takada, Y. Yamashita, S. Ishikawa, S.-i. Fujiwara, H. Watanabe, K. Kurashina and H. Hatanaka, *Nature*, 2007, **448**, 561-567.
4. F. R. Jazii, Z. Najafi, R. Malekzadeh, T. P. Conrads, A. A. Ziaee, C. Abnet, M. Yazdznbod, A. A. Karkhane and G. H. Salekdeh, *World J. Gastroenterol.*, 2006, **12**, 7104-7112.
5. R. D. Gascoyne, L. Lamant, J. I. Martin-Subero, V. S. Lestou, N. L. Harris, H.-K. Müller-Hermelink, J. F. Seymour, L. J. Campbell, D. E. Horsman and I. Auvigne, *Blood*, 2003, **102**, 2568-2573.
6. R. Roskoski Jr, *Pharmacol. Res.*, 2013, **68**, 68-94.
7. R. Crescenzo and G. Inghirami, *Curr. Opin. Pharmacol.*, 2015, **23**, 39-44.
8. Y.-J. Bang, *Arch. Pathol. Lab. Med.*, 2012, **136**, 1201-1204.
9. W.-C. Wang, H.-Y. Shiao, C.-C. Lee, K.-S. Fung and H.-P. Hsieh, *MedChemComm*, 2014, **5**, 1266-1279.
10. Y. L. Choi, M. Soda, Y. Yamashita, T. Ueno, J. Takashima, T. Nakajima, Y. Yatabe, K. Takeuchi, T. Hamada and H. Haruta, *N. Engl. J. Med.*, 2010, **363**, 1734-1739.
11. T. Sasaki, K. Okuda, W. Zheng, J. Butrynski, M. Capelletti, L. Wang, N. S. Gray, K. Wilner, J. G. Christensen and G. Demetri, *Cancer Res.*, 2010, **70**, 10038-10043.
12. T. Sasaki, J. Koivunen, A. Ogino, M. Yanagita, S. Nikiforow, W. Zheng, C. Lathan, J. P. Marcoux, J. Du and K. Okuda, *Cancer Res.*, 2011, **71**, 6051-6060.
13. R. C. Doebele, A. B. Pilling, D. Aisner, T. G. Kutateladze, A. T. Le, A. J. Weickhardt, K. L. Kondo, D. J. Linderman, L. E. Heasley and W. A. Franklin, *Clin. Cancer Res.*, 2012, **18**, 1472-1482.
14. J. F. Gainor and A. T. Shaw, *J. Clin. Oncol.*, 2013, **31**, 3987-3996.
15. S. Shin, S. Mah, S. Hong and H. Park, *J. Chem. Inf. Model.*, 2016, **56**, 802-810.
16. S. Mah, J. H. Park, H.-Y. Jung, K. Ahn, S. Choi, H. S. Tae, K. H. Jung, J. K. Rho, J. C. Lee and S.-S. Hong, *J. Med. Chem.*, 2017, **60**, 9205-9221.
17. M. Kawaguchi, T. Okabe, S. Okudaira, K. Hanaoka, Y. Fujikawa, T. Terai, T. Komatsu, H. Kojima, J. Aoki and T. Nagano, *J. Am. Chem. Soc.*, 2011, **133**, 12021-12030.
18. L. C. Kenmogne, R. Maltais and D. Poirier, *Bioorg. Med. Chem. Lett.*, 2016, **26**, 2179-2183.
19. J. J. Yim, M. Tholen, A. Klaassen, J. Sorger and M. Bogyo, *Mol. Pharm.*, 2017, **15**, 750-758.
20. H. Yao, G. Wei, Y. Liu, H. Yao, Z. Zhu, W.-C. Ye, X. Wu, J. Xu and S. Xu, *ACS Med. Chem. Lett.*, 2018, **9**, 1030-1034.
21. J. C. McGrath, S. Arribas and C. J. Daly, *Trends Pharmacol. Sci.*, 1996, **17**, 393-399.
22. J. G. Baker, I. P. Hall and S. J. Hill, *Br. J. Pharmacol.*, 2003, **139**, 232-242.
23. X.-h. Liu and G. D. Prestwich, *Bioorg. Med. Chem. Lett.*, 2004, **14**, 2137-2140.
24. C. M. Crane, J. Kaiser, N. L. Ramsden, S. Lauw, F. Rohdich, W. Eisenreich, W. N. Hunter, A. Bacher and F. Diederich, *Angew. Chem. Int. Ed.*, 2006, **45**, 1069-1074.
25. J. Son, J.-J. Lee, J.-S. Lee, A. Schüller and Y.-T. Chang, *ACS Chem. Biol.*, 2010, **5**, 449-453.
26. D. Kim, H. Lee, H. Jun, S.-S. Hong and S. Hong, *Bioorg. Med. Chem.*, 2011, **19**, 2508-2516.
27. J. Dhuguru, W. Liu, W. G. Gonzalez, W. M. Babinchak, J. Miksovska, R. Landgraf and J. N. Wilson, *J. Org. Chem.*, 2014, **79**, 4940-4947.
28. V. M. Yenugonda, T. B. Deb, S. C. Grindrod, S. Dakshanamurthy, Y. Yang, M. Paige and M. L. Brown, *Bioorg. Med. Chem.*, 2011, **19**, 2714-2725.
29. M. Min and S. Hong, *Chem. Commun.*, 2012, **48**, 9613-9615.
30. M. Min, B. Kim and S. Hong, *Org. Biomol. Chem.*, 2012, **10**, 2692-2698.
31. D. Kim, M. Min and S. Hong, *Chem. Commun.*, 2013, **49**, 4021-4023.
32. M. Min, Y. Kim and S. Hong, *Chem. Commun.*, 2013, **49**, 196-198.
33. Y. Moon, Y. Kim, H. Hong and S. Hong, *Chem. Commun.* 2013, **49**, 8323-8325.
34. Y. Kim, Y. Moon, D. Kang and S. Hong, *Org. Biomol. Chem.*, 2014, **12**, 3413-3422.
35. J. Hoult and M. Paya, *Gen. Pharmacol.*, 1996, **27**, 713-722.
36. I. Kostova, *Curr. Med. Chem. Anticancer Agents*, 2005, **5**, 29-46.
37. R. Dayam, R. Gundla, L. Q. Al-Mawsawi and N. Neamati, *Med. Res. Rev.*, 2008, **28**, 118-154.
38. P. T. Thuong, T. M. Hung, T. M. Ngoc, D. T. Ha, B. S. Min, S. J. Kwack, T. S. Kang, J. S. Choi and K. Bae, *Phytother. Res.*, 2010, **24**, 101-106.
39. S.-Y. Bai, X. Dai, B.-X. Zhao and J.-Y. Miao, *RSC Adv.*, 2014, **4**, 19887-19890.
40. S. Emami and S. Dadashpour, *Eur. J. Med. Chem.*, 2015, **102**, 611-630.
41. B. D. Wagner, *Molecules*, 2009, **14**, 210-237.
42. J. J. Cui, M. Tran-Dubé, H. Shen, M. Nambu, P.-P. Kung, M. Pairish, L. Jia, J. Meng, L. Funk and I. Botrous, *J. Med. Chem.*, 2011, **54**, 6342-6363.
43. H. Sakamoto, T. Tsukaguchi, S. Hiroshima, T. Kodama, T. Kobayashi, T. A. Fukami, N. Oikawa, T. Tsukuda, N. Ishii and Y. Aoki, *Cancer Cell*, 2011, **19**, 679-690.
44. T. W. Johnson, P. F. Richardson, S. Bailey, A. Brooun, B. J. Burke, M. R. Collins, J. J. Cui, J. G. Deal, Y.-L. Deng and D. Dinh, *J. Med. Chem.*, 2014, **57**, 4720-4744.
45. When cell viability assay against Ba/F3 EML4-ALK WT (EA WT) was conducted, representative compounds **5a** and **6a** inhibited the cell growth in a dose-dependent manner (**5a**: IC_{50} = 6.8 μM, **6a**: IC_{50} = 28.2 μM).

View Article Online
DOI: 10.1039/C8OB02874E

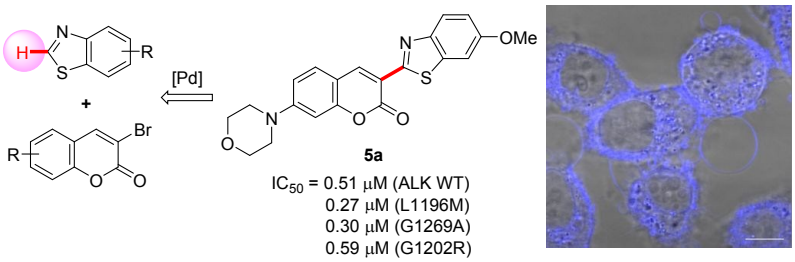

Coumarin-based ALK inhibitors were identified as a new template for the development of novel fluorescent ALK inhibitors, which can be tracked using microscopy techniques.